


## Article

# IBF-R Regulates IRE1 $\alpha$ Post-Translational Modifications and ER Stress in High-Fat Diet-Induced Obese Mice

Hwa-Young Lee <sup>1,2</sup>, Geum-Hwa Lee <sup>2</sup>, Young Yoon <sup>3</sup>, The-Hiep Hoang <sup>2,4</sup>  and Han-Jung Chae <sup>2,5,\*</sup>

- <sup>1</sup> Department of Pharmacology, Institute of New Drug Development, Medical School, Jeonbuk National University, Jeonju 54896, Jeollabuk-do, Korea; youngat84@gmail.com
- <sup>2</sup> Non-Clinical Evaluation Center, Biomedical Research Institute, Jeonbuk National University Hospital, Jeonju 54907, Jeollabuk-do, Korea; heloin@jbnu.ac.kr (G.-H.L.); drhiep.ydhue@gmail.com (T.-H.H.)
- <sup>3</sup> Imsil Cheese & Food Research Institute, Doin 2-gil, Seongsu-myeon, Imsil-gun 55918, Jeollabuk-do, Korea; kuburi79@icf.re.kr
- <sup>4</sup> Research Institute of Clinical Medicine, Jeonbuk National University-Biomedical Research Institute, Jeonbuk National University Hospital, Jeonju 54907, Jeollabuk-do, Korea
- <sup>5</sup> School of Pharmacy, Jeonbuk National University, Jeonju 54896, Jeollabuk-do, Korea
- \* Correspondence: hjchael@jbnu.ac.kr; Tel.: +82-63-270-3092

**Abstract:** Obesity is a global health issue linked to the heightened risk of several chronic diseases. *Rhus verniciflua* (RV) is a traditional food supplement used for a range of pharmacological effects such as antitumor, antioxidant,  $\alpha$ -glucosidase inhibitory effects, hepatitis, and arthritis. Despite the traditional medicinal values, scientific evidence for its application in obesity is inadequate and unclear. Thus, this investigation was designed to evaluate the anti-obesity effects of IBF-R, an RV extract, using a high-fat diet (HFD) model. The study has six groups: chow diet group; chow diet with 80 mg/kg IBF-R; HFD group; IBF-R group with 20, 40, and 80 mg/kg. IBF-R supplementation significantly regulated the weight gain than the HFD fed mice. Further, IBF-R supplementation lowered the expressions of adipogenic transcription factors such as SREBP-1c, C/EBP $\alpha$ , FAS, and PPAR- $\gamma$  in white adipose tissue (WAT) of diet-induced obese mice. In addition, IBF-R supplementation reduced the lipogenic gene expression while enhancing genes was related to fatty acid oxidation. Obesity is linked to redox-based post-translational modifications (PTMs) of IRE1 $\alpha$  such as S-nitrosylation, endoplasmic reticulum (ER) stress, and chronic metabolic inflammation. The administration of IBF-R inhibits these PTMs. Notably, IBF-R administration significantly enhanced the expression of AMPK and sirtuin 1 in WAT of HFD-fed mice. Together, these findings reveal the IRE1 $\alpha$  S-nitrosylation-inflammation axis as a novel mechanism behind the positive implications of IBF-R on obesity. In addition, it lays a firm foundation for the development of *Rhus verniciflua* extract as a functional ingredient in the food and pharmaceutical industries.

**Keywords:** obesity; *Rhus verniciflua*; high-fat diet; S-nitrosylation; ER stress; adipogenesis



**Citation:** Lee, H.-Y.; Lee, G.-H.; Yoon, Y.; Hoang, T.-H.; Chae, H.-J. IBF-R Regulates IRE1 $\alpha$  Post-Translational Modifications and ER Stress in High-Fat Diet-Induced Obese Mice. *Nutrients* **2022**, *14*, 217. <https://doi.org/10.3390/nu14010217>

Received: 7 December 2021

Accepted: 31 December 2021

Published: 4 January 2022

**Publisher's Note:** MDPI stays neutral with regard to jurisdictional claims in published maps and institutional affiliations.



**Copyright:** © 2022 by the authors. Licensee MDPI, Basel, Switzerland. This article is an open access article distributed under the terms and conditions of the Creative Commons Attribution (CC BY) license (<https://creativecommons.org/licenses/by/4.0/>).

## 1. Introduction

Obesity is abnormal fat accumulation in adipose tissues and characterized by body mass index (BMI) higher than 30 kg/m<sup>2</sup> and is associated with multiple chronic diseases such as type 2 diabetes, cardiovascular disorders, and different types of cancers [1]. White adipose tissue (WAT) executes a variety of metabolic tasks under physiological conditions. However, WAT loses its functional capabilities with obesity negatively affecting its storage of surplus energy. This process leads to ectopic fat accumulation in several tissues influencing metabolic homeostasis [2]. Thus, developing strategies against lipogenesis and lipid dysmetabolism in obesity and associated diseases has potential therapeutic benefits [3]. Furthermore, previous investigations demonstrate that visceral adipose tissue has higher inflammatory and immunological cells than subcutaneous adipose tissue. Hence, regulating

visceral adipose tissue development by lowering lipogenesis and enhancing lipid oxidation could be a promising approach to treat obesity and associated metabolic dysfunction.

Obesity is a complicated health condition involving multiple molecular mechanisms. Aging impairs endoplasmic reticulum (ER) chaperones and foldases, affecting protein folding capabilities [4]. In addition, redox signaling imbalances or abnormal redox-associated post-translational modifications (PTMs) alter protein structure or function, resulting in pathogenic diseases. However, the underlying mechanisms underpinning obesity-related redox imbalance, and ER proteostasis dysfunction, as well as their significance in disease progression, remain unknown. Obese adipose tissues are prone to stressful conditions such as hypoxia, ER stress, and oxidant stress [5,6]. Recent reports suggest up-regulation of ER stress markers such as phosphorylated PERK (p-PERK), phosphorylated  $\alpha$ -subunit of eukaryotic translational initiating factor 2 (eIF2 $\alpha$ ), and BiP in liver and adipose tissues of high-fat-diet (HFD) mice [6]. Moreover, multiple investigations have found enhanced free fatty acids (FFAs) during obesity, potentially inducing ER stress in adipocytes and other cells [7,8]. However, underlying mechanisms that induce ER stress in adipose tissue or the relationship between ER stress and chronic inflammation during obesity are unclear. Here, we discovered that excessive reactive nitrogen species (RNS) build up during obesity, causing nitro-oxidative stress and triggering cysteine oxidation. These processes induce alterations in ER membrane protein, IRE1 $\alpha$ . Further, the functioning of IRE1 $\alpha$  is influenced by S-nitrosylation of IRE1 $\alpha$ .

*Rhus verniciflua* (RV) is a traditional food supplement used for its medicinal values for centuries in Eastern Asia. The use of RV was demonstrated to have several pharmacological effects, including  $\alpha$ -glucosidase inhibitory effects, antioxidant, antitumor, anti-inflammatory, and antibacterial effects [9–11]. The abundance of flavonoids and polyphenols such as fisetin, sulfuretin, quercetin, fustin, and butein in RV are thought to be responsible for these pharmacological actions. Additionally, modifications in hepatic metabolism and related dysfunctions are strongly linked to RV [12,13]. Still, scientific evidence for its beneficial effects on obesity is inadequate and unclear. Thus, we hypothesized that RV could protect against obesity by modulating obesity-related instability in the ER function. In this study, IBF-R, RV extract is extracted through water extraction as it is more popular than other methods. Here, efforts are put to investigate the potential impact and mechanism behind the beneficial effects of IBF-R on obesity.

## 2. Materials and Methods

### 2.1. The Preparation of IBF-R

IBF-R, RV extract was extracted as described previously [14]. Finely powdered RV was hot air dried, boiled, condensed, and lyophilized to obtain dried RV extract (IBF-R). The yield of IBF-R was close to 4%. The quality control was performed using standard compounds such as Fisetin as described before [15].

### 2.2. Animal Studies

Male C57BL/6J mice (6 weeks old) were procured from Orient Science Co. (Seongnam, Korea). All the animals were kept in well-ventilated cages at  $22 \pm 2$  °C under a standard light-dark cycle. All the mice used in this study were acclimatized for a week prior to use. Later, 7 weeks old mice were randomly selected and separated into six groups, with 8 mice in each group. NCD mice receiving water were assigned as Group 1. NCD mice receiving 80 mg/kg of IBF-R were assigned as Group 2. HFD-fed mice receiving water were assigned as Group 3. Group 4 received 20 mg/kg IBF-R, Group 5 received 40 mg/kg IBF-R and Group 6 received 80 mg/kg IBF-R. The experimental diet was continued for up to 12 weeks. At the end of the experiment, all the animals were sacrificed to collect samples. Collected whole blood was stored immediately at 2 °C for 30 min and centrifuged to separate the serum. All the samples were maintained at  $-80$  °C until use. The animal tests were performed by following the Jeonbuk National University hospital's animal care and use committee guidelines (CUH-IACUC-2019-10).

### 2.3. Biochemical Analysis

All the biochemical tests were performed using commercial kits. Whole blood was collected using EDTA vacutainers. Serum was separated by centrifuging the blood at  $3000 \times g$  10 min at 4 °C. Triglyceride (TG, AM1575K) and total cholesterol (TC, AM202K) were detected using commercial test kits from Asan Pharmaceutical, Seoul, Republic of Korea. Plasma levels of adiponectin (CSB-E07272m, CUSABIO, Houston, TX, USA) and leptin (CSB-E04650m, CUSABIO, Houston, TX, USA) were determined using commercial sandwich ELISA kits. The absorbance at 450 nm was detected using Multiskan SkyHigh microplate spectrophotometer (Thermo Fisher Scientific, Inc., Waltham, MA, USA). The unknown sample concentration (ng/mL) was determined from the standard curve.

### 2.4. Immunoblotting

Immunoblotting was performed as described earlier [15]. All the immunoblots were probed with relevant antibodies. Antibodies used in this study are AMP-activated kinase (AMPK, #2532) and phosphorylation of AMP-activated kinase (p-AMPK, P-2535) (Cell Signaling Technologies, Inc., Danvers, MA, USA) and sterol regulatory element-binding protein (SREBP-1c, sc-36553), peroxisome proliferator-activated receptor  $\gamma$  (PPAR- $\gamma$ ), CCAAT/enhancer-binding protein  $\alpha$  (C/EBP1 $\alpha$ , sc-166258), fatty acid synthase (FAS, sc-74540), sirtuin 1 (SIRT1, sc-74465),  $\beta$ -actin (sc-47778, Santa Cruz, Biotechnologies, Inc., Santa Cruz, CA, USA).

### 2.5. Oxyblot Assay

Tissue carbonylated protein was measured via OxyBlot Protein oxidation Kit (Millipore, Billerica, MA, USA) as per guidelines set by the producer. Briefly, samples were incubated 1:1 in 2,4-dinitrophenylhydrazine (DNPH) and added 2-mercaptoethanol for protein denaturing. Later, a neutralization reagent was used to cease the reaction, and samples were loaded for immunoblotting as described in previous sections.

### 2.6. Histological Analysis and Immunohistochemistry (IHC)

The liver and WAT were dissected and fixed with 10% formalin. Later, paraffin-embedded tissue blocks were sectioned 4  $\mu$ m and stained with H&E. Similarly, for IHC, formalin-fixed, paraffin-embedded tissues were processed as described previously [15].

### 2.7. Reverse Transcription Polymerase Chain Reaction (RT-PCR)

Total RNA from tissue was isolated with TRIzol (Invitrogen, Carlsbad, CA, USA). Extraction was performed with 1  $\mu$ g of RNA with oligo dT primers. SYBR premix Ex Taq kit (TaKaRa Bio Inc., Shiga, Kusatsu, Japan) was used for quantitative PCR. Quantification was performed by a comparative cycle threshold (Ct) method, and the resultant product was normalized to  $\beta$ -actin expression.

### 2.8. Lipid Peroxidation Measurement

Adipose tissue lipid peroxidation was measured with OxiSelect™ TBARS Assay Kit (#STA-330, Cell Biolabs, Inc. San Diego, CA, USA), as per the guidelines set by the manufacturer. Briefly, samples were incubated with lysis buffer and allowed to react with thiobarbituric acid (TBA). Cooled samples were centrifuged to collect the supernatant, and absorbance was measured at 532 nm.

### 2.9. Detection of High Molecular Weight Complex (HMWC)

HMWC's were detected by following previous reports [16]. Homogenized whole adipose tissues were used to detect HMWC of Protein Disulfide Isomerase (PDI, ADI-SPA-891-F, Enzo Life Sciences, Inc., Farmingdale, NY, USA). Washed adipose tissue supplemented with 1mM phenylmethylsulfonyl fluoride (PMSF) is lysed, homogenized, sonicated, cleared, and quantified. Next, about 50  $\mu$ g of total protein was separated under non-reducing conditions using 8% polyacrylamide gels.

2.10. Detection of S-Nitrosylation

Detection of S-nitrosylation was performed with Pierce™ S-nitrosylation kit (#90105; Thermo Scientific, Waltham, MA, USA) as per the guidelines set by the manufacturer. This test enables the detection of protein S-nitrosocysteine (CySNO) PTMs. Briefly, S-nitrosylated proteins were treated with MMTS to restrict free sulfhydryls, followed by protein precipitation with acetone to eliminate MMTS. Then, S-nitrosylated proteins were modified with biotin (0.2 mM biotin-HPDP, Thermo Scientific, Waltham, MA, USA) in HPDP buffer for 1h at 4 °C in the dark. Next, biotinylated proteins were purified using acetone followed by pulling down in neutralizing buffer with streptavidin-agarose (GE healthcare, Waukesha, WI, USA). The beads were washed in neutralizing buffer with 600 mM NaCl, and then samples were eluted with an elution buffer containing 20 mM HEPES, 100 mM NaCl, 1 mM EDTA, 100 mM 2-ME. Western blot was employed to detect were detected by chemiluminescence (Bio-Rad, Hercules, CA, USA). The proteins of interest were measured with relevant antibodies.

2.11. Data Analysis

Data are shown as mean ± SEM. To compare multiple groups, one-way ANOVA with Tukey post hoc was applied. All statistical analyses were performed with GraphPad Prism version 8.0 (GraphPad Software, San Diego, CA, USA). A level of significance was set at  $p \leq 0.05$ .

3. Results

3.1. IBF-R Controls Body Weight Gain and Its Influence on Metabolic Profile in HFD Induced Obese Mice

First, C57BL/6J mice were fed with 60% HFD for 12 weeks with or without IBF-R supplementation. IBF-R supplementation regulated the weight gain than the HFD fed mice (Figure 1a,b). Further, a micro-CT scan showed higher visceral adipose tissue in the HFD group than in the NCD group. Contrastingly, HFD fed mice with IBF-R supplementation dose-dependently reduced fat accumulation (Figure 1c). This observation was verified with the measurement of volume with the micro-CT program, where it indicated dose-dependent lower orbital fat volume (%) with IBF-R treatment (Figure 1d). Similar observations were recorded with respect to the weight of the liver, eWAT, and iWAT (Figure 1e–g). Interestingly, food intake in all the groups remained the same (Supplementary Figure S1a).

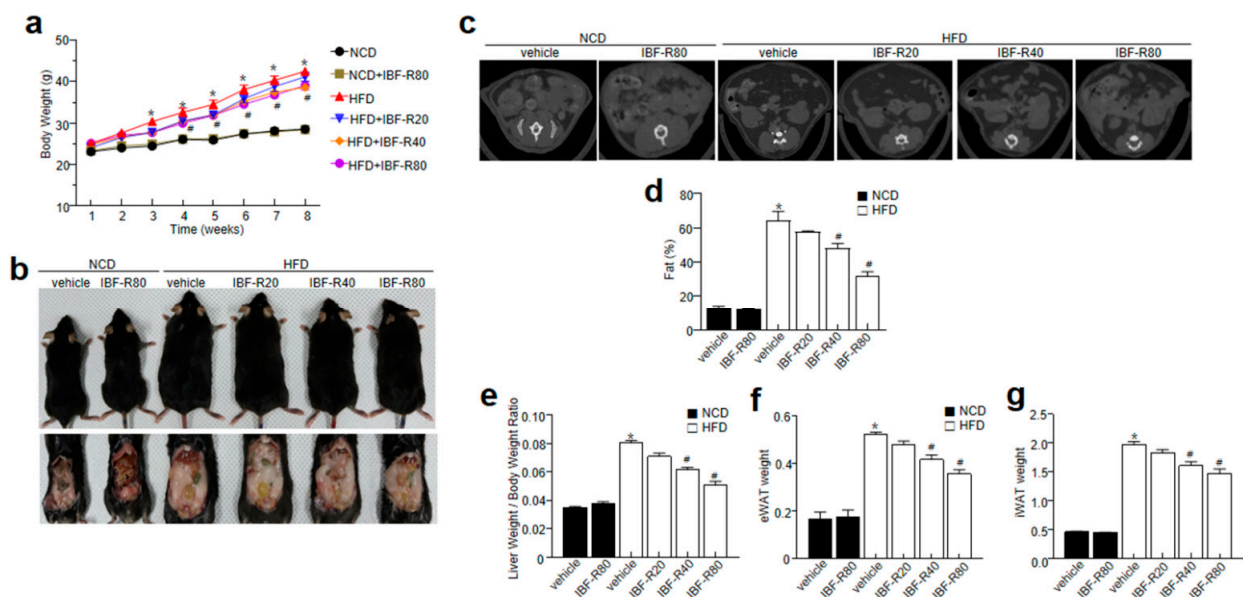


**Figure 1.** Influence of IBF-R on body weight and fat mass. Mice were fed with NCD or HFD with vehicle or IBF-R (20, 40, or 80 mg/kg). All the animals were gavaged daily for 12 weeks. (a) Variations



in body weight at predetermined time points. (b) Representative images of HFD mice after 12 weeks of IBF-R supplementation. (c) Representative Micro-CT images were obtained using Skyscan1076 micro-CT scanner. (d) Quantification of fat mass with Skyscan1076 micro-CT scanner at the end of the experiment. (e–g) Measurement of epididymal white adipose tissue (eWAT), inguinal white adipose tissue (iWAT) and liver weight. Data are shown as mean ± SEM ( $n = 10$ , \*  $p < 0.05$  vs. NCD + vehicle, #  $p < 0.05$  vs. HFD + vehicle).

### 3.2. IBF-R Controls Biochemical Characteristics and Ameliorates Hepatic Lipid Accumulation in HFD Induced Obese Mice

Lipid contents were scrutinized to evaluate the influence of IBF-R on lipid homeostasis. NCD and HFD mice without IBF-R treatment showed considerably higher serum TG and TC levels, while IBF-R demonstrated significantly lower TG and TC levels (Figure 2a,b). IBF-R played a significant role in restoring blood glucose levels (Supplementary Figure S1b). Moreover, IBF-R supplementation improved adiponectin and lowered leptin levels dose-dependently (Figure 2c,d). Histological analysis of the liver revealed increased deposition of lipid droplets in HFD fed mice while IBF-R treatment drastically cut down the accumulation of lipid droplets (Figure 2e).

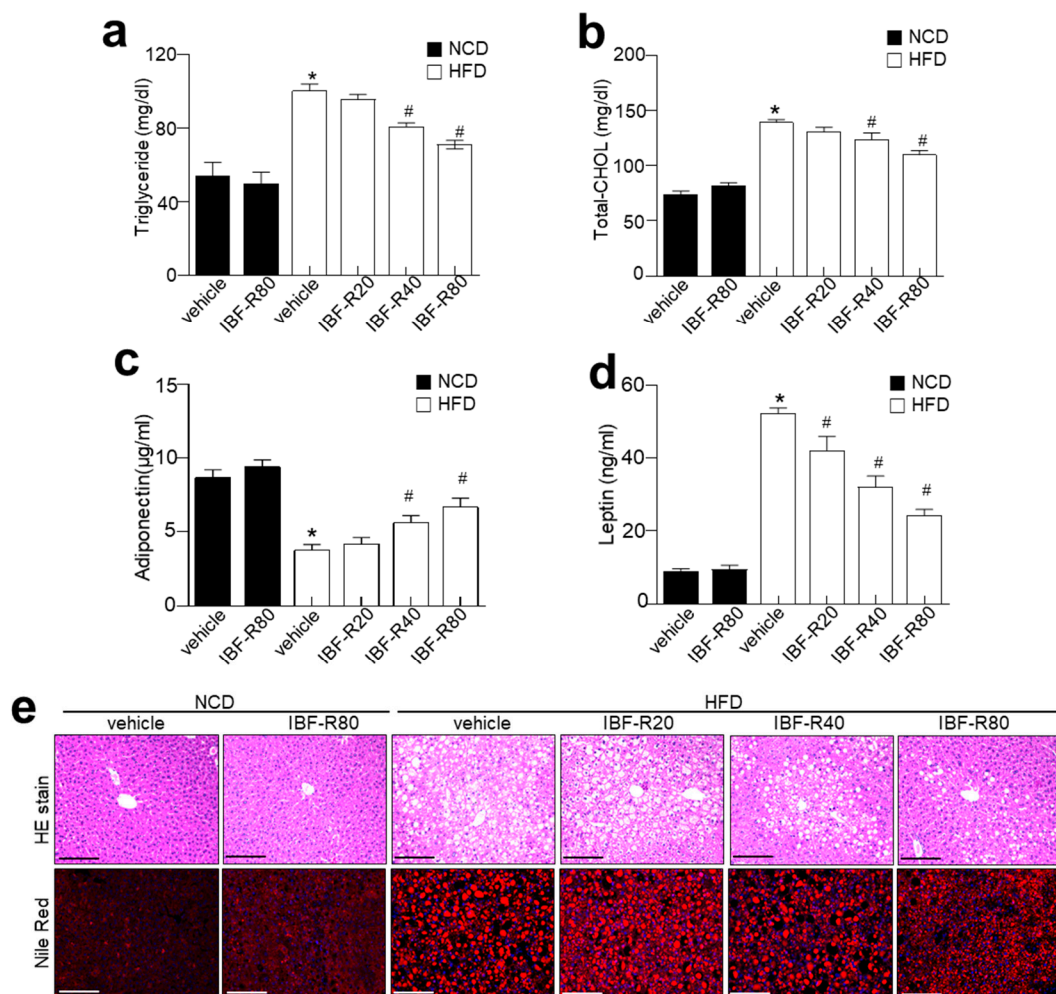


**Figure 2.** Influence of IBF-R serum biochemicals profile and lipid accumulation. Levels of triglyceride (a), total cholesterol (b), adiponectin (c), and leptin (d). (e) Representative images of liver sections stained with H&E (upper) and Nile Red stain (lower). Scale bars = 50 µm. Data are shown as mean ± SEM ( $n = 10$ , \*  $p < 0.05$  vs. NCD + vehicle, #  $p < 0.05$  vs. HFD + vehicle).

### 3.3. IBF-R Regulates Adipogenesis through Redox-Mediated Post-Translational Modifications (PTMs) of IRE1 $\alpha$ and ER Stress Response in HFD Induced Obese Mice

IRE1 $\alpha$  is involved in ER homeostasis by causing a translational frameshift by starting unusual splicing of the mRNA encoding X-box-binding protein 1 (XBP1). It creates spliced XBP1 (sXBP1), a strong transcription factor that controls the expression of genes that encode ER chaperones [4] and proteins influencing phospholipid synthesis and afresh lipogenesis [17]. We observed enhanced IRE1 $\alpha$  phosphorylation, sXBP-1, c-Jun N-terminal kinase (JNK) activation, GRP78, and CHOP expression, indicating preserved activation of the canonical ER stress sensors (Figure 3a,b). In response to ER stress, ER stress axis-based UPR is generated where IRE1 $\alpha$  activates XBP-1 via unusual splicing of XBP-1 mRNA, followed by translocation of sXBP1 into the nucleus for the induction of chaperone proteins restoring ER homeostasis [18]. In Figure 3c, the IRE1 $\alpha$  executor signaling “the nuclear translocation of sXBP-1” was slightly observed in HFD group. In contrast, the reduced translocation was significantly recovered in the IBF-R-treated groups (quantified in Figure 3d), suggesting a distinct molecular mechanism against metabolic disorders and obesity than recognized ER stress axis “IRE1 $\alpha$  phosphorylation-sXBP-1 activation.

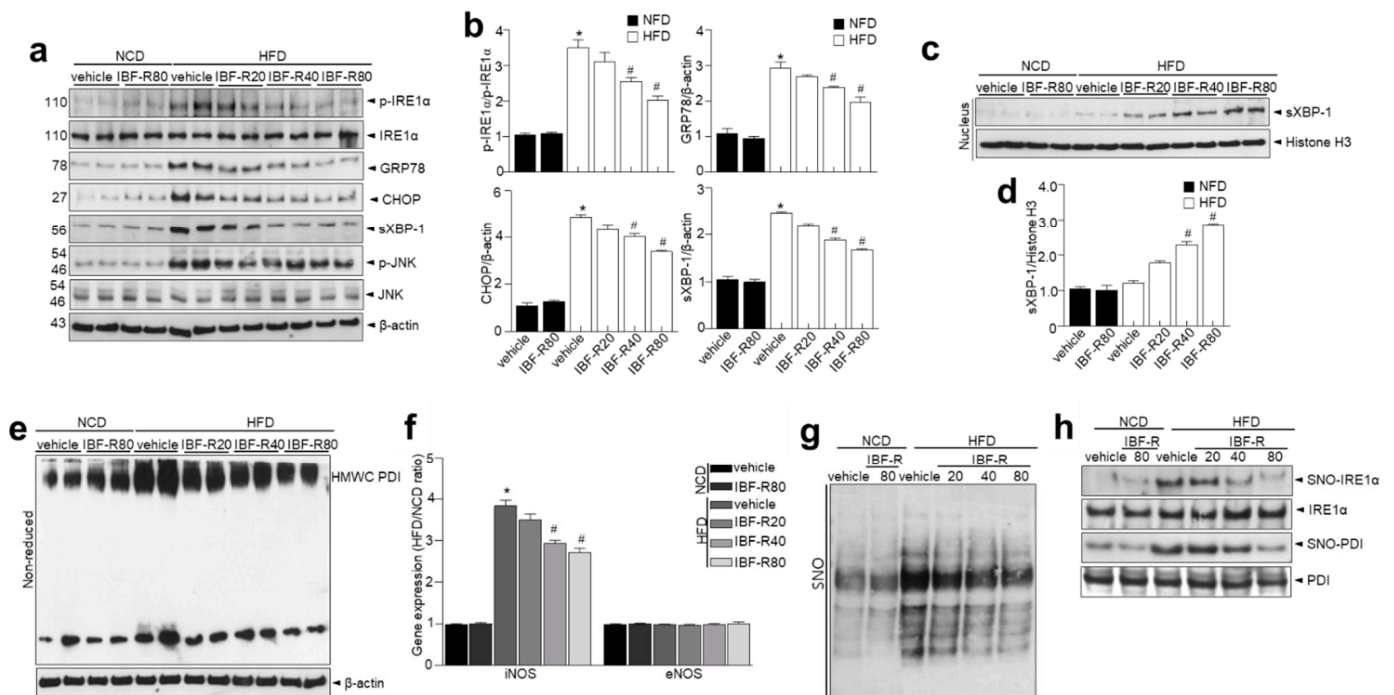


**Figure 3.** IBF-R diminish ER stress and IRE1 $\alpha$  S-nitrosylation of axis in HFD model. (a) Immunoblotting of p-IRE1 $\alpha$ , IRE1 $\alpha$ , GRP78, CHOP, sXBP-1, and  $\beta$ -actin expressions in eWAT. (b) Quantitative analysis of proteins. (c,d) sXBP1 expressions at the nuclear level from each group and quantitative analysis. (e) eWAT lysate was examined for PDI in HMWCs on non-reducing gels. (f) iNOS and eNOS mRNAs were measured in eWAT by qRT-PCR. (g) General S-nitrosylation (SNO) profile in eWAT of HFD mice and NCD controls. (h) Specific SNO proteins in the eWAT of HFD mice and NCD controls. S-nitrosylated proteins were purified with biotin-switch assay and detected by immunoblotting. Data are shown as mean  $\pm$  SEM ( $n = 10$ , \*  $p < 0.05$  vs. NCD + vehicle, #  $p < 0.05$  vs. HFD + vehicle). eWAT; epididymal white adipose tissue.

Hence, we examined the ER quality control state through ER quality-control system [19]. Disruptions in the folding of client proteins do not allow it to attain mature conformation such as HMWC [20]. These multiprotein complexes were enhanced in HFD conditions (Figure 3e), which IBF-R attenuated. In obesity showing ER stress conditions, we asserted that obesity-induced and phosphorylation-independent modifications in IRE1 $\alpha$  might suppress ribonuclease activity selectively. We observed a substantial rise in iNOS

expression in HFD conditions, which coincides with the decrease in the sXBP1 activity “the nuclear translocation of sXBP-1” in adipose tissue of obese mice (Figure 3f) [16]. This coincidence represents an obesity model featuring chronic metabolic inflammation [21–23], whereas IBF-R significantly suppressed the iNOS level. Besides, other NO enzymes and endothelial NOS (eNOS) expression levels were comparable in the NCD and HFD conditions. S-nitrosylation, a protein modification involving covalent binding of nitrogen monoxide group to the thiol side chain of cysteine residues, appeared to be the underlying molecular process for active posttranslational regulation of proteins such as PDI [24]. In this study, we evaluated general protein S-nitrosylation (SNO) changes in the adipose tissues of NCD and HFD mice using biotin switch assay [25,26]. Protein S-nitrosylation was greatly increased in the HFD condition but significantly reduced in the IBF-R-treated conditions. (Figure 3g). Next, S-nitrosylated proteins were extracted from the adipose tissues of HFD and NCD mice to evaluate the influence of varying nitrosylation status affecting ER function. In addition, proteins critical to ER stress and adaptive responses were detected. These evaluations showed that multiple ER chaperones such as IRE1 $\alpha$  and PDI demonstrated enhanced S-nitrosylation (Figure 3h) in HFD conditions while IBF-R decreased S-nitrosylation. These findings show that S-nitrosylation targets IRE1 $\alpha$  raising the potential changes in the functioning of IRE1 $\alpha$  in obese adipose tissue.

#### 3.4. IBF-R Controls Adipogenesis-Linked Proteins in Adipose Tissues in HFD Induced Obese Mice

H&E staining demonstrated that the IBF-R-treated condition is highly efficient in reducing the size and diameter of the adipocytes than the HFD group (Figure 4a,b). Later, the expressions of adipogenic transcription factors in eWAT were analyzed to clarify the contribution of reduced epididymal WAT (eWAT) in IBF-R-treated mice. Moreover, IBF-R significantly lowered the protein expressions of C/EBP $\alpha$ , SREBP1, PPAR $\gamma$ , and FAS than in the HFD group (Figure 4c–f). Lipid accumulation in adipose cells is due to enhanced lipogenesis and reduced  $\beta$ -oxidation [22]. Furthermore, markers of fatty acid oxidation and lipogenesis in eWAT and liver were evaluated to determine the molecular mechanisms of lowering eWAT mass upon IBF-R supplementation. Moreover, we scrutinized the expression of adipogenic transcription factors in eWAT to understand the process responsible for eWAT mass reduction upon IBF-R administration. The supplementation of IBF-R showed reduced SREBP1, PPAR $\gamma$ , C/EBP $\alpha$ , and FAS levels than the HFD group (Figure 4g–k). Similarly to eWAT, in liver tissues, HFD increased the adipogenic protein expression of SREBP1, PPAR $\gamma$ , C/EBP $\alpha$ , and FAS compared to the NCD group, whereas IBF-R administration significantly downregulated SREBP1, PPAR $\gamma$ , C/EBP $\alpha$ , and FAS compared to the HFD group (Supplementary Figure S2).

In addition, p-AMPK was relatively less expressed in the HFD group than in the NCD group, while IBF-R significantly enhanced p-AMPK expression (Figure 4l,m). Next, SIRT1 expression was then examined to see if it was involved in regulating genes linked to adipogenic, lipogenic, and fatty acid oxidation. Interestingly, SIRT1 was greatly expressed in the IBF-R group than in the HFD group (Figure 4l,m). Together, these observations suggest that IBF-R controls the weight of eWAT and liver via modifications in adipogenesis-associated transcription factors.

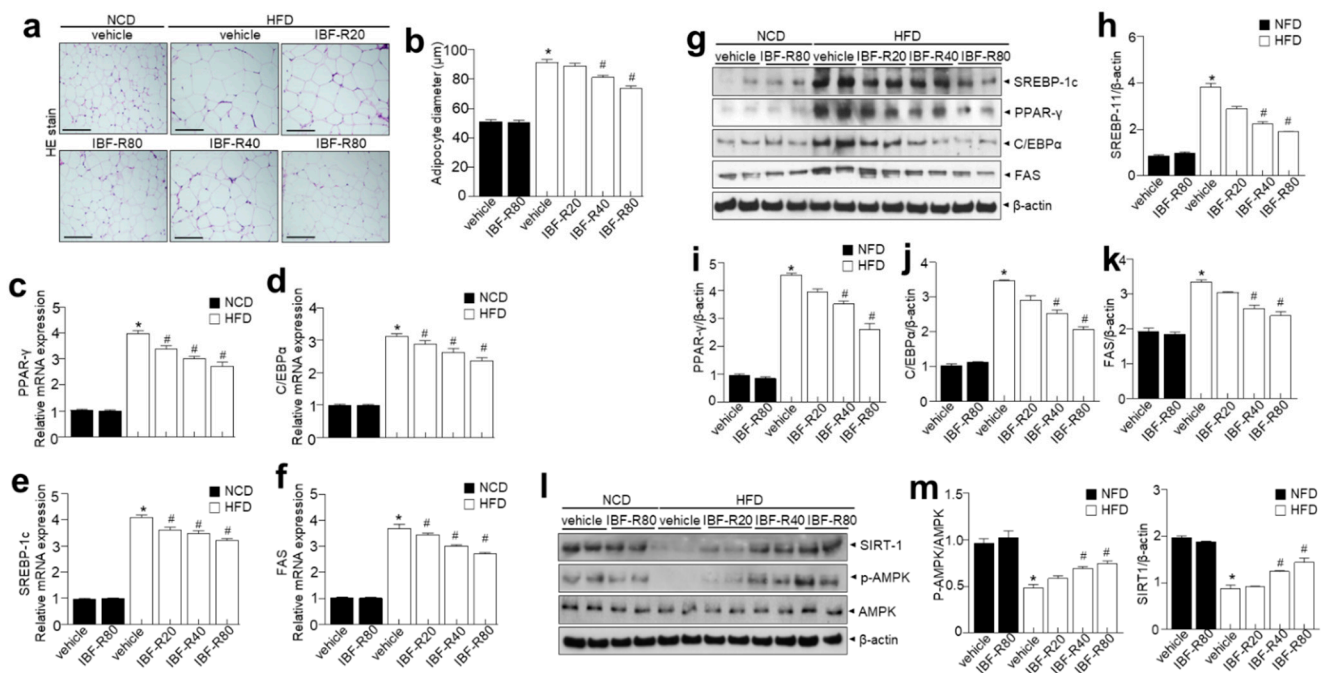


**Figure 4.** IBF-R determines adipose tissue expansion and adipogenic factors in eWAT. (a) H&E staining in eWAT. Scale bar = 50 μm. (b) The mean diameter of adipocytes in eWAT. (c–f) C/EBPα, PPAR-γ, FAS and SREBP-1c were measured in eWAT by qRT-PCR. (g) Immunoblotting of PPAR-γ, C/EBPα, SREBP-1c, FAS, and β-actin expressions in eWAT. (h–k) Quantification of protein expressions. (l,m) Immunoblotting of p-AMPK, AMPK, SIRT-1, and β-actin expressions in eWAT and respective quantitative analysis. Data are shown as mean ± SEM ( $n = 10$ , \*  $p < 0.05$  vs. NCD + vehicle, #  $p < 0.05$  vs. HFD + vehicle). eWAT; epididymal white adipose tissue.

#### 4. Discussion

This study revealed the potential influence of IBF-R on obesity and extrapolated mechanisms behind positive implications on the adipose tissue of HFD mice. IBF-R treatment inhibited HFD-induced iNOS production as well as elevation of IRE1α S-nitrosylation, a master ER stress response signal, and associated fat accumulation and adipogenesis. Our findings suggest the IRE1α S-nitrosylation-inflammation axis as a novel mechanism to explain how IBF-R treatment regulates obesity. In addition, the study reveals that AMPK-SIRT1 activation is an IBF-R dependent mechanism in the obesity model.

IBF-R regulated body weight increase and its associated lipid dysmetabolism with which adipocyte differentiation is related. Obesity is characterized by excessive fat deposition that heavily impacts weight gain. IBF-R treatment significantly controlled the increase in body weight and fat accumulation without affecting food consumption. Furthermore, total cholesterol, triglyceride, and LDL-chol levels were considerably lower in the IBF-R treatment group. Several transcriptional factors such as PPARγ and C/EBP family proteins mediate adipogenesis [27]. The expressions of C/EBPβ and C/EBPδ stimulates the expressions of C/EBPα and PPARγ, which are considered critical positive regulators of adipogenesis during the early stages of adipocyte development. In addition, PPARγ is the key regulator during adipocyte development and differentiation [28]. Cells with PPARγ deficiency halt the development of adipocytic cells. As a result, they could not develop as matured adipocytes although unconventionally expressed of other pro-adipogenic factors [29]. In this investigation, IBF-R supplementation exhibited downregulation of PPARγ and C/EBP along with its downstream FAS than the HFD condition. Other transcriptional factors involved in adipogenesis modulation include CREB1 and SREBP1c. Specifically, SREBP1c is required for adipocyte differentiation and can stimulate PPAR and FAS expression [30]. However, IBF-R significantly reduced SREBP1c and FAS in the HFD model. These



observations back up the concept that IBF-R treatment reduced adipogenesis in eWAT of HFD induced obese mice.

IBF-R regulated IRE1 $\alpha$  post-translational modifications (PTMs), leading to ER homeostasis and its related lipid homeostasis. S-nitrosylation of IRE1 $\alpha$  suppresses its endoribonuclease activity, preventing sXBP1 synthesis, thereby preventing downstream targets such as decreased ER chaperones, malfunctioned autophagy or ERAD failure, all of which are required to preserve ER homeostasis. Obesity is related to increased iNOS-induced metaflammation and reduced XBP1 processing [31], similar to study findings in the HFD-induced obesity model (Figure 3c). Obesity, insulin resistance (IR), and diabetic nephropathy exhibit faulty nuclear translocation of sXBP1 [32–34], where the link within sXBP1 and PI3K regulatory subunits (p85 $\alpha$  and p85 $\beta$ ) was disrupted, exacerbating disease etiology [34,35]. Study data suggest that IBF-R passes IRE1 $\alpha$ -mediated XBP1 splicing, relying on redox-mediated PTMs of IRE1 $\alpha$  into SNO, facilitating modifications of IRE1 $\alpha$ . Contentious stimulation of SNO decides whether IRE1 RNase splicing activity is activated or inhibited, giving critical signals that decide cell adaptation or death. IBF-R demonstrated its potentials in regulating adipogenesis by sustaining redox-linked PTMs and ER homeostasis. Moreover, previously, we have demonstrated that severe redox-mediated PTMs of IRE1 $\alpha$  impairs ER function and sustain ER stress in aging/metabolic disorder models suggesting the S-nitrosylation of IRE1 $\alpha$  affects its endoribonuclease activity, thereby impairs sXBP1, leading to inflammation [16]. In addition, the increased iNOS-induced metaflammation is associated with impaired XBP1 processing in obesity [31]. A defective nuclear translocation of sXBP1 has been reported in metabolic disorders such as obesity and diabetes [32,33], indicating the potential use of IRE1 $\alpha$  modifications, i.e., the IBF-R might prevent or control obesity.

The other finding is that IBF-R enhanced the AMPK-SIRT1 axis controlling adipogenesis in HFD model. In addition, we observed IBF-R stimulated AMPK expression influencing fatty acid metabolism and adipose tissue development (Figure 4). Additionally, AMPK activation is linked to a reduction in lipid accumulation [36]. Furthermore, it also inhibits FAS and alleviates fatty acid oxidation by phosphorylating ACC [37]. A769662, an activator of AMPK, reduces lipid droplets, PPAR $\gamma$ , and C/EBP [38]. Due to obesity, AMPK becomes inactive necessitating external stimuli to activate AMPK. SIRT1 is a key member of the sirtuin family that plays a vital role in improving the fighting capacity of the cell against stress in multiple ways, including regulation of aging, metabolic activity and apoptosis, and ER stress [39]. SIRT1 deacetylates XBP1 blocking its transcriptional activity, enhancing ER stress-linked programmed cell death, and decreasing translational inhibition dependent on PERK-eIF2 in mice [40,41]. Hence, SIRT1 is considered a negative regulator of the ER stress response. Here, IBF-R was observed to be regaining SIRT1, p-AMPK, which controls SREBP-1c signaling and the associated ER stress response (Figure 4l,m). These findings suggest that IBF-R protects against obesity via reduced adipocyte formation and lipogenesis in the eWAT, potentially with enhanced AMPK/SIRT1 activation linked with ER stress.

In summary, the study revealed that supplementation of IBF-R cut down the risks of obesity in the HFD model via repressing fat accumulation in the WAT. Concerning molecular mechanisms, treatment with IBF-R upholds AMPK-SIRT1 signaling and modulates SREBP1-ER stress. Collectively, investigation adds strong evidence on the health benefits of RV extract and lays a firm foundation for the development of RV extract as a functional ingredient in the food and pharmaceutical industry.

**Supplementary Materials:** The following are available online at <https://www.mdpi.com/article/10.3390/nu14010217/s1>, Figure S1: Influence of IBF-R on food intake and blood glucose levels. Figure S2: IBF-R determines adipogenic factors in liver tissue.

**Author Contributions:** Conceptualization, H.-Y.L.; data curation, H.-Y.L., G.-H.L. and T.-H.H.; resources, Y.Y.; writing—original draft, H.-Y.L.; writing—review and editing, H.-J.C. All authors have read and agreed to the published version of the manuscript.

**Funding:** This study was supported by the Imsil Cheese and Food Research Institute, Imsil-gun, Jeolla-buk-do, 55908, Korea. This research was supported by a grant of the Korea Health Technology R&D Project through the Korea Health Industry Development Institute (KHIDI), funded by the Ministry of Health and Welfare, Korea (Grant Number: HI20C1933).

**Institutional Review Board Statement:** Not applicable.

**Informed Consent Statement:** Not applicable.

**Data Availability Statement:** The data presented in this study are available upon request from the corresponding author.

**Conflicts of Interest:** The authors declare no conflict of interest.

## References

1. Gadde, K.M.; Martin, C.K.; Berthoud, H.R.; Heymsfield, S.B. Obesity: Pathophysiology and Management. *J. Am. Coll. Cardiol.* **2018**, *71*, 69–84. [[CrossRef](#)] [[PubMed](#)]
2. Kusminski, C.M.; Bickel, P.E.; Scherer, P.E. Targeting adipose tissue in the treatment of obesity-associated diabetes. *Nat. Rev. Drug Discov.* **2016**, *15*, 639–660. [[CrossRef](#)] [[PubMed](#)]
3. Serra, D.; Mera, P.; Malandrino, M.I.; Mir, J.F.; Herrero, L. Mitochondrial fatty acid oxidation in obesity. *Antioxid. Redox Signal.* **2013**, *19*, 269–284. [[CrossRef](#)]
4. Brown, M.K.; Naidoo, N. The endoplasmic reticulum stress response in aging and age-related diseases. *Front. Physiol.* **2012**, *3*, 263. [[CrossRef](#)]
5. Furukawa, S.; Fujita, T.; Shimabukuro, M.; Iwaki, M.; Yamada, Y.; Nakajima, Y.; Nakayama, O.; Makishima, M.; Matsuda, M.; Shimomura, I. Increased oxidative stress in obesity and its impact on metabolic syndrome. *J. Clin. Investig.* **2004**, *114*, 1752–1761. [[CrossRef](#)]
6. Ozcan, U.; Cao, Q.; Yilmaz, E.; Lee, A.H.; Iwakoshi, N.N.; Ozdelen, E.; Tuncman, G.; Gorgun, C.; Glimcher, L.H.; Hotamisligil, G.S. Endoplasmic reticulum stress links obesity, insulin action, and type 2 diabetes. *Science* **2004**, *306*, 457–461. [[CrossRef](#)] [[PubMed](#)]
7. Cnop, M.; Foufelle, F.; Velloso, L.A. Endoplasmic reticulum stress, obesity and diabetes. *Trends Mol. Med.* **2012**, *18*, 59–68. [[CrossRef](#)]
8. Jiao, P.; Ma, J.; Feng, B.; Zhang, H.; Diehl, J.A.; Chin, Y.E.; Yan, W.; Xu, H. FFA-induced adipocyte inflammation and insulin resistance: Involvement of ER stress and IKKbeta pathways. *Obesity* **2011**, *19*, 483–491. [[CrossRef](#)]
9. Jung, C.H.; Jun, C.Y.; Lee, S.; Park, C.H.; Cho, K.; Ko, S.G. Rhus verniciflua stokes extract: Radical scavenging activities and protective effects on H<sub>2</sub>O<sub>2</sub>-induced cytotoxicity in macrophage RAW 264.7 cell lines. *Biol. Pharm. Bull.* **2006**, *29*, 1603–1607. [[CrossRef](#)]
10. Kim, K.H.; Moon, E.; Choi, S.U.; Kim, S.Y.; Lee, K.R. Polyphenols from the bark of Rhus verniciflua and their biological evaluation on antitumor and anti-inflammatory activities. *Phytochemistry* **2013**, *92*, 113–121. [[CrossRef](#)]
11. Nam, T.G.; Lee, B.H.; Choi, H.K.; Mansur, A.R.; Lee, S.G.; Kim, D.O. Rhus verniciflua Stokes Extract and Its Flavonoids Protect PC-12 Cells against H<sub>2</sub>O<sub>2</sub>-Induced Cytotoxicity. *J. Microbiol. Biotechnol.* **2017**, *27*, 1090–1097. [[CrossRef](#)]
12. Lee, J.H.; Lee, H.J.; Lee, H.J.; Choi, W.C.; Yoon, S.W.; Ko, S.G.; Ahn, K.S.; Choi, S.H.; Ahn, K.S.; Lieske, J.C.; et al. Rhus verniciflua Stokes prevents cisplatin-induced cytotoxicity and reactive oxygen species production in MDCK-I renal cells and intact mice. *Phytomedicine Int. J. Phytother. Phytopharm.* **2009**, *16*, 188–197. [[CrossRef](#)]
13. Lee, M.S.; Kim, J.S.; Cho, S.M.; Lee, S.O.; Kim, S.H.; Lee, H.J. Fermented Rhus verniciflua Stokes Extract Exerts an Antihepatic Lipogenic Effect in Oleic-Acid-Induced HepG2 Cells via Upregulation of AMP-Activated Protein Kinase. *J. Agric. Food Chem.* **2015**, *63*, 7270–7276. [[CrossRef](#)]
14. Lee, H.Y.; Lee, G.H.; Yoon, Y.; Chae, H.J. R. verniciflua and E. ulmoides Extract (ILF-RE) Protects against Chronic CCl<sub>4</sub>-Induced Liver Damage by Enhancing Antioxidation. *Nutrients* **2019**, *11*, 382. [[CrossRef](#)]
15. Hoang, T.H.; Yoon, Y.; Park, S.A.; Lee, H.Y.; Peng, C.; Kim, J.H.; Lee, G.H.; Chae, H.J. IBF-R, a botanical extract of Rhus verniciflua controls obesity in which AMPK-SIRT1 axis and ROS regulatory mechanism are involved in mice. *J. Funct. Foods* **2021**, *87*, 104804. [[CrossRef](#)]
16. Bhattarai, K.R.; Kim, H.-K.; Chaudhary, M.; Ur Rashid, M.M.; Kim, J.; Kim, H.-R.; Chae, H.-J. TMBIM6 regulates redox-associated posttranslational modifications of IRE1 $\alpha$  and ER stress response failure in aging mice and humans. *Redox Biol.* **2021**, *47*, 102128. [[CrossRef](#)] [[PubMed](#)]
17. Bonomini, F.; Rodella, L.F.; Rezzani, R. Metabolic syndrome, aging and involvement of oxidative stress. *Aging Dis.* **2015**, *6*, 109–120. [[CrossRef](#)] [[PubMed](#)]
18. Calton, M.; Zeng, H.; Urano, F.; Till, J.H.; Hubbard, S.R.; Harding, H.P.; Clark, S.G.; Ron, D. IRE1 couples endoplasmic reticulum load to secretory capacity by processing the XBP-1 mRNA. *Nature* **2002**, *415*, 92–96. [[CrossRef](#)]
19. Anelli, T.; Sitia, R. Protein quality control in the early secretory pathway. *EMBO J.* **2008**, *27*, 315–327. [[CrossRef](#)] [[PubMed](#)]
20. Kenche, H.; Baty, C.J.; Vedagiri, K.; Shapiro, S.D.; Blumental-Perry, A. Cigarette smoking affects oxidative protein folding in endoplasmic reticulum by modifying protein disulfide isomerase. *FASEB J. Off. Publ. Fed. Am. Soc. Exp. Biol.* **2013**, *27*, 965–977. [[CrossRef](#)] [[PubMed](#)]

21. Nakamura, T.; Furuhashi, M.; Li, P.; Cao, H.; Tuncman, G.; Sonenberg, N.; Gorgun, C.Z.; Hotamisligil, G.S. Double-stranded RNA-dependent protein kinase links pathogen sensing with stress and metabolic homeostasis. *Cell* **2010**, *140*, 338–348. [[CrossRef](#)]
22. Zhang, X.; Zhang, G.; Zhang, H.; Karin, M.; Bai, H.; Cai, D. Hypothalamic IKKbeta/NF-kappaB and ER stress link overnutrition to energy imbalance and obesity. *Cell* **2008**, *135*, 61–73. [[CrossRef](#)] [[PubMed](#)]
23. Lumeng, C.N.; Saltiel, A.R. Inflammatory links between obesity and metabolic disease. *J. Clin. Investig.* **2011**, *121*, 2111–2117. [[CrossRef](#)]
24. Uehara, T.; Nakamura, T.; Yao, D.; Shi, Z.Q.; Gu, Z.; Ma, Y.; Masliah, E.; Nomura, Y.; Lipton, S.A. S-nitrosylated protein-disulphide isomerase links protein misfolding to neurodegeneration. *Nature* **2006**, *441*, 513–517. [[CrossRef](#)] [[PubMed](#)]
25. Derakhshan, B.; Wille, P.C.; Gross, S.S. Unbiased identification of cysteine S-nitrosylation sites on proteins. *Nat. Protoc.* **2007**, *2*, 1685–1691. [[CrossRef](#)] [[PubMed](#)]
26. Jaffrey, S.R.; Snyder, S.H. The biotin switch method for the detection of S-nitrosylated proteins. *Sci. STKE* **2001**, *2001*, p11. [[CrossRef](#)]
27. Ali, A.T.; Hochfeld, W.E.; Myburgh, R.; Pepper, M.S. Adipocyte and adipogenesis. *Eur. J. Cell Biol.* **2013**, *92*, 229–236. [[CrossRef](#)] [[PubMed](#)]
28. Ghaben, A.L.; Scherer, P.E. Adipogenesis and metabolic health. *Nat. Rev. Mol. Cell Biol.* **2019**, *20*, 242–258. [[CrossRef](#)]
29. Rosen, E.; Eguchi, J.; Xu, Z. Transcriptional targets in adipocyte biology. *Expert Opin. Ther. Targets* **2009**, *13*, 975–986. [[CrossRef](#)]
30. Khalilpourfarshbafi, M.; Gholami, K.; Murugan, D.D.; Abdul Sattar, M.Z.; Abdullah, N.A. Differential effects of dietary flavonoids on adipogenesis. *Eur. J. Nutr.* **2019**, *58*, 5–25. [[CrossRef](#)]
31. Yang, L.; Calay, E.S.; Fan, J.; Arduini, A.; Kunz, R.C.; Gygi, S.P.; Yalcin, A.; Fu, S.; Hotamisligil, G.S. S-Nitrosylation links obesity-associated inflammation to endoplasmic reticulum dysfunction. *Science* **2015**, *349*, 500–506. [[CrossRef](#)] [[PubMed](#)]
32. Park, S.W.; Zhou, Y.; Lee, J.; Lu, A.; Sun, C.; Chung, J.; Ueki, K.; Ozcan, U. The regulatory subunits of PI3K, p85alpha and p85beta, interact with XBP-1 and increase its nuclear translocation. *Nat. Med.* **2010**, *16*, 429–437. [[CrossRef](#)] [[PubMed](#)]
33. Winnay, J.N.; Boucher, J.; Mori, M.A.; Ueki, K.; Kahn, C.R. A regulatory subunit of phosphoinositide 3-kinase increases the nuclear accumulation of X-box-binding protein-1 to modulate the unfolded protein response. *Nat. Med.* **2010**, *16*, 438–445. [[CrossRef](#)]
34. Madhusudhan, T.; Wang, H.; Dong, W.; Ghosh, S.; Bock, F.; Thangapandi, V.R.; Ranjan, S.; Wolter, J.; Kohli, S.; Shahzad, K.; et al. Defective podocyte insulin signalling through p85-XBP1 promotes ATF6-dependent maladaptive ER-stress response in diabetic nephropathy. *Nat. Commun.* **2015**, *6*, 6496. [[CrossRef](#)]
35. Bhattarai, K.R.; Riaz, T.A.; Kim, H.R.; Chae, H.J. The aftermath of the interplay between the endoplasmic reticulum stress response and redox signaling. *Exp. Mol. Med.* **2021**, *53*, 151–167. [[CrossRef](#)] [[PubMed](#)]
36. Bijland, S.; Mancini, S.J.; Salt, I.P. Role of AMP-activated protein kinase in adipose tissue metabolism and inflammation. *Clin. Sci.* **2013**, *124*, 491–507. [[CrossRef](#)] [[PubMed](#)]
37. Fullerton, M.D.; Galic, S.; Marcinko, K.; Sikkema, S.; Pulinilkunnil, T.; Chen, Z.-P.; O'Neill, H.M.; Ford, R.J.; Palanivel, R.; O'Brien, M.; et al. Single phosphorylation sites in Acc1 and Acc2 regulate lipid homeostasis and the insulin-sensitizing effects of metformin. *Nat. Med.* **2013**, *19*, 1649–1654. [[CrossRef](#)]
38. Zhou, Y.; Wang, D.; Zhu, Q.; Gao, X.; Yang, S.; Xu, A.; Wu, D. Inhibitory Effects of A-769662, a Novel Activator of AMP-Activated Protein Kinase, on 3T3-L1 Adipogenesis. *Biol. Pharm. Bull.* **2009**, *32*, 993–998. [[CrossRef](#)]
39. Feng, K.; Ge, Y.; Chen, Z.; Li, X.; Liu, Z.; Li, X.; Li, H.; Tang, T.; Yang, F.; Wang, X. Curcumin Inhibits the PERK-eIF2 $\alpha$ -CHOP Pathway through Promoting SIRT1 Expression in Oxidative Stress-induced Rat Chondrocytes and Ameliorates Osteoarthritis Progression in a Rat Model. *Oxidative Med. Cell. Longev.* **2019**, *2019*, 8574386. [[CrossRef](#)]
40. Prola, A.; Pires Da Silva, J.; Guilbert, A.; Lecru, L.; Piquereau, J.; Ribeiro, M.; Mateo, P.; Gressette, M.; Fortin, D.; Boursier, C.; et al. SIRT1 protects the heart from ER stress-induced cell death through eIF2 $\alpha$  deacetylation. *Cell Death Differ.* **2017**, *24*, 343–356. [[CrossRef](#)]
41. Chou, X.; Ding, F.; Zhang, X.; Ding, X.; Gao, H.; Wu, Q. Sirtuin-1 ameliorates cadmium-induced endoplasmic reticulum stress and pyroptosis through XBP-1s deacetylation in human renal tubular epithelial cells. *Arch. Toxicol.* **2019**, *93*, 965–986. [[CrossRef](#)] [[PubMed](#)]